Manifold Parametrization of the Left Ventricle for a Statistical Modelling of its Complete Anatomy

D Gil and J. Garcia-Barnes and A. Hernandez-Sabate and E. Marti [a]

[a]Computer Vision Center and Department of Computer Science, Univ. Autonoma de Barcelona, Bellaterra, Spain.

ABSTRACT

Distortion of Left Ventricle (LV) external anatomy is related to some dysfunctions, such as hypertrophy. The architecture of myocardial fibers determines LV electromechanical activation patterns as well as mechanics. Thus, their joined modelling would allow the design of specific interventions (such as peacemaker implantation and LV remodelling) and therapies (such as resynchronization). On one hand, accurate modelling of external anatomy requires either a dense sampling or a continuous infinite dimensional approach, which requires non-Euclidean statistics. On the other hand, computation of fiber models requires statistics on Riemannian spaces. Most approaches compute separate statistical models for external anatomy and fibers architecture.

In this work we propose a general mathematical framework based on differential geometry concepts for computing a statistical model including, both, external and fiber anatomy. Our framework provides a continuous approach to external anatomy supporting standard statistics. We also provide a straightforward formula for the computation of the Riemannian fiber statistics. We have applied our methodology to the computation of complete anatomical atlas of canine hearts from diffusion tensor studies. The orientation of fibers over the average external geometry agrees with the segmental description of orientations reported in the literature.

1. INTRODUCTION

The most common approach for the modelling of shape variations in anatomical structures are Point Distribution Models (PDM).[1] PDM are discrete approaches which are based on the statistical modelling of a set of anatomical landmarks describing the geometry of the anatomical structure. By its linear formulation, PDM complexity and computational cost is very low which makes them useful in many computer vision applications (e.g. face segmentation). However, in the case of anatomical structures, the ability of PDM to capture the variability of finer details requires a massive selection of landmarks. This has lead to designing computational methods[2] for the automatic generation of huge sets of landmarks over anatomical structures. The maximum resolution in the representation of shapes can be achieved by considering continuous models. Such models explore the variability of shapes by performing statistics directly over the diffeomorphic mappings required to register anatomies to a reference one.[3,4] A main inconvenience is that the space of diffeomorphic mappings is an infinite dimensional space without vector space structure. This forces the development of special statistical models with a complex formulation.

The modelling of the LV gross anatomy has been widely addressed. However, the inclusion of its internal architecture is a relatively new issue. Although the approximate helical architecture of the heart has been known for decades, a complete and consistent anatomical description of cardiac structure has not been achieved yet. This issue is currently one of the most controversial aspects of the modern cardiology and, several conceptual architectural models have been proposed[5] so far. There is, however, a general consensus that cardiac architecture plays a critical role in many functional aspects of the heart such as electrical propagation.[6] In addition, it is also accepted that myocardium may undergo architectural alterations in many heart diseases.[7] It follows that fiber architecture models should be taken into account in electrical and mechanical simulations applied to the planning of patient-specific therapies.[8]

Further author information:
D.G.: E-mail: debora@cvc.uab.cat, Telephone: +34 93 581 2301
J.G.B.: E-mail: jaumegb@cvc.uab.cat, Telephone: +34 93 581 2301

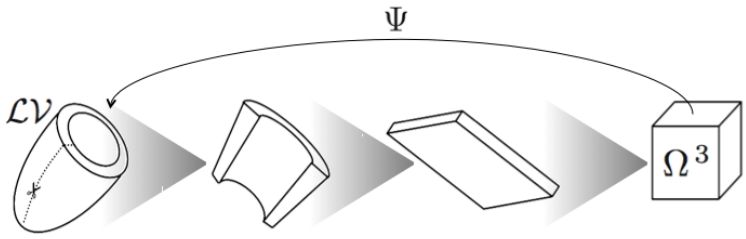

Figure 1. Unfolding process of the LV that provides a parametrization, Ψ, between a rectangular domain and $\mathcal{LV}$.

Recently, Diffusion Tensor Imaging (DTI), a technique for measuring the self-diffusion of protons in fibrous tissue, has emerged as a powerful new tool for the rapid measurement of the whole cardiac architecture at a reasonable spatial resolution (approximately $300 \times 300 \times 1000\,\mu m^3$). DTI directly provides a 3D description of the fiber architecture as well as its external anatomy by means of data volumes. Architectural data is given by a tensor (at each point) which diagonalizes in three orthogonal eigenvectors. Histological studies have demonstrated that the primary eigenvector correlates well to myofiber direction.[9] In contrast to traditional techniques such as dissection and histology, a main advantage of DTI is that it provides digital data sets prone to be statistically studied. This has motivated active research in the extraction of statistical models involving fiber architecture aspects. For instance, scalar descriptors of their orientation.[4,10] Few researchers, however, have addressed the creation of statistical models (atlases) of cardiac fiber architecture so far. This is mainly due to the fact that diffusion tensors are symmetric positive definite matrices that do not belong to any vector space. Thus, classical Euclidean multivariate statistics are not consistent. In,[11] Riemmanian geometry, based on either affine-invariant or Log-Euclidean metrics,[12] have been used for the computation of first and second order statistics of the whole diffusion tensors.

Following this trend, the goal of the present work is to create a complete statistical model of the LV including both, the gross anatomy and the fibers distribution. In order to achieve this, we present a framework based on Differential Geometry concepts (manifold parameterization), which is simple and computationally efficient. We call this framework Normalzed Parametric Domain (NPD).

2. NPD FRAMEWORK

The keypoint of the NPD framework relies on a particluar parameterization of the LV volume in the sense of differentiable manifolds.[13] As suggested in,[14] this parameterization must be done in such a way that equivalent anatomical locations (in different subjects) are assigned the same tuple of normalized (between 0 and 1) circumferential, longitudinal and radial parameters. This leads to a mapping that relates the unitary cube $\Omega^3 = [0,1] \times [0,1] \times [0,1]$ to the LV (which will be noted by $\mathcal{LV}$). We call Ω^3 Normalized Parametric Domain, which gives the name to the whole framework.

Notice that in order to handle both, the gross anatomy and the fibers architecture, this formulation is very useful. On one hand, the image of the mapping, $\Psi(\Omega^3)$, provides the gross geometry of the LV. On the other hand, since equivalent locations (across different subjects) have been labelled with the same parametric tuple, any quantity measured over the LV (in these subjects) can be mapped back to the same location in Ω^3 for comparison purposes.[15] In this case we say that both LVs are implicitly registered in the Normalized Parametric Domain. Figure 2 shows two LVs ($\mathcal{LV}_i$ and $\mathcal{LV}_j$) implicitly registered. Vectorial quantities defined on equivalent locations are moved to the same parametric location in Ω^3 where comparison becomes feasible.

The Jacobian of the parametric map:

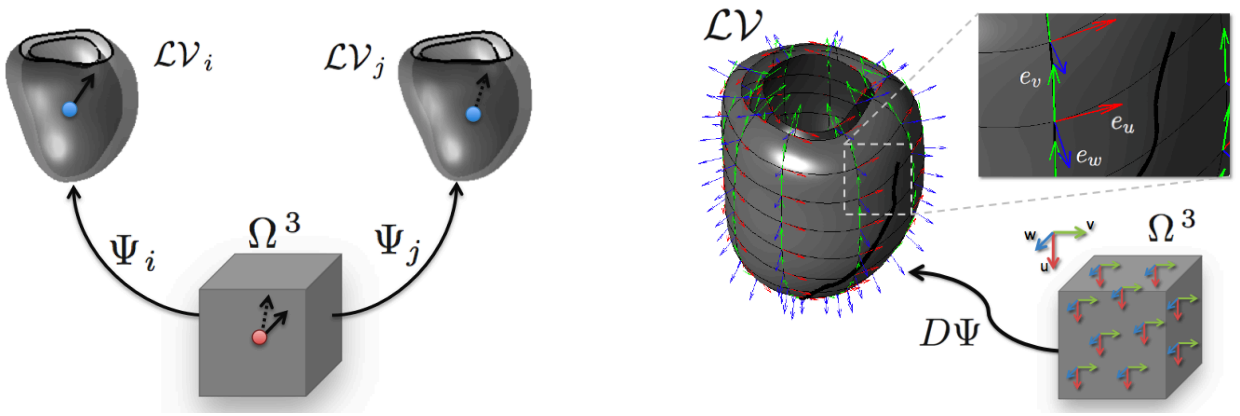

(a) (b)

Figure 2. a) Two LVs ($\mathcal{LV}_i$ and $\mathcal{LV}_j$) implicitly registered in Ω^3. That is, equivalent anatomical locations (blue dots in $\mathcal{LV}_i$ and $\mathcal{LV}_j$) have the same parameter configuration (red dot in Ω^3). b) The differential $D\Psi$, defines a local reference, at each point of $\mathcal{LV}$, describing its anatomy.

$$D\Psi(u,v,w) = (\nabla_u \Psi(p), \nabla_v \Psi(p), \nabla_w \Psi(p)) = \begin{pmatrix} \frac{\partial \Psi_1}{\partial u} & \frac{\partial \Psi_1}{\partial v} & \frac{\partial \Psi_1}{\partial w} \\ \frac{\partial \Psi_2}{\partial u} & \frac{\partial \Psi_2}{\partial v} & \frac{\partial \Psi_2}{\partial w} \\ \frac{\partial \Psi_3}{\partial u} & \frac{\partial \Psi_3}{\partial v} & \frac{\partial \Psi_3}{\partial w} \end{pmatrix} \tag{1}$$

defines at each point $p \in \mathcal{LV}$ a non orthogonal reference of unitary vectors $\{e_u(p), e_w(p), e_w(p)\}$:

$$e_u = \frac{\nabla_u \Psi}{\|\nabla_u \Psi\|_2}, e_v = \frac{\nabla_v \Psi}{\|\nabla_v \Psi\|_2}, e_w = \frac{\nabla_w \Psi}{\|\nabla_w \Psi\|_2} \tag{2}$$

describing the local geometry of the $\mathcal{LV}$ volume. Figure 2 (a) shows the description of $\mathcal{LV}$ local geometry given by $D\Psi(u,v,w)$. We observe that the reference vectors (2) are tangent to $\mathcal{LV}$ parametric curves, so that in the NPD they correspond to the axis defined by the parametric coordinates (u,v,w). Notice that Ψ can be regarded as a change of coordinates tailored for the geometry of each subject. Intuitively, this parameterization unfolds ("straightens") the geometry of $\mathcal{LV}$ as shown in Figure 1. Unlike standard changes of coordinates (either spheroidal[16] or cylindrical[10]) in the cartesian image volume, our local reference is able to capture the subject-specific $\mathcal{LV}$ geometry (given by the parametrization of the volumetric manifold[13]).

Besides being a convinient representation for jointly handling gross anatomy and fiber architecture, the NPD framework enjoys several advantages over approaches registering volumes to a reference $\mathcal{LV}$ domain in cartesian coordinates. For instance, the NPD framework allows a straightforward definition of neighborhoods adapted to $\mathcal{LV}$ subject-specific anatomy since parametric curves are completely addapted to the LV geometry.[15] It follows that local operations such as interpolation or smoothing can be done taking into account the underlying geometry of the LV.

2.1 Gross Anatomy Modelling

In order to define the parametric map we use a B-Spline formulation:

$$\Psi(u,v,w) = \sum_{i=1}^{M_u} \sum_{j=1}^{M_v} \sum_{k=1}^{M_w} R_i(u) S_j(v) T_k(w) P_{ijk} \tag{3}$$

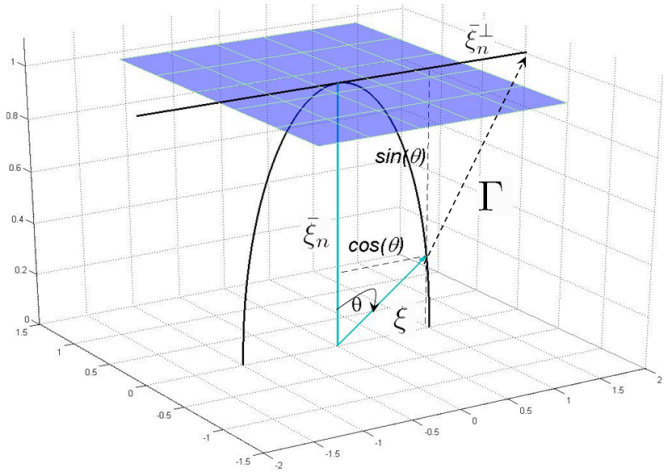

Figure 3. Sketch of the definition of the exponential map onto S^2.

This representation enables our NPD framework to continuously describe the geometry of the LV with a finite number of parameters: the control points. It follows that the set of parametric maps has a vectorial structure. Taking advantage of this fact, we use the control points to model LV shape variations as in PDM.

A main requirement for the PDM to be statistically meaningful, is that the selected landmarks must be consistent. That is, they must represent the same anatomical location for any subject. Since in our case control points play the role of anatomical landmarks, they should influence equivalent anatomical areas for any subject. Since equivalent anatomical point share the same parameters, this consistency condition is fulfilled.

Given the geometry (codified by the parametric maps) of N subjects:

$$\Psi_n(u,v,w) = \sum_{i=1}^{M_u}\sum_{j=1}^{M_v}\sum_{k=1}^{M_w} R_{i,n}(u)S_{j,n}(v)T_{k,n}(w)P_{ijk,n}, \qquad n = 1,\cdots,N \tag{4}$$

we gather the control points of each of them in a sigle vector called observation:

$$\mathbf{P}_n = (P^x_{100,n}, P^y_{100,n}, P^z_{100,n}, \cdots, P^x_{M_uM_vM_w,n}, P^y_{M_uM_vM_w,n}, P^z_{M_uM_vM_w,n}) \tag{5}$$

Next, all the observations are aligned using Procrustes Analysis[17] and the mean and covariance matrices are computed in order to obtain the PDM.[1]

2.2 Fiber Modelling

The tangent application $D\Psi$ maps vectors, V, expressed in cartesian image volume coordinates into the NPD.[13] By linearity of the tangent application, the mapping is given by the decomposition of V in the local reference (2). Such components can be mapped to the NPD for statistical analysis. Therefore, we use $D\Psi$ to map the unitary eigenvectors obtained from parameterized DTI volumes, to Ω^3. Since we are only interested in fiber directions, we normalize and reorient the components (in the local references) in order them to belong to the upper (positive) semi sphere (S^{2+}). The DTI vectors normalized and reoriented in Ω^3 will be noted by ξ.

(S^{2+}) is a manifold and, computing statistics, on manifolds is, by no means, a trivial issue.[12,18,19] This is due to the fact that the formulation of descriptive statistics (mean and standard deviation) in an Euclidean (vector) space, relies on the fact that the addition is a well defined operation. In contrast, manifolds do not present vector space structure and the addition is not well defined. In order to compute statistics on manifolds, the concept of mean and variance should be generalized.[11,20–22] The key point for their extension relies on the fact that the mean is, indeed, the value that minimizes the function of the square distances

$$min_{\bar{\xi}\in\mathbb{R}^m}\frac{1}{N}\sum_{n=1}^{N}\|\xi_n-\bar{\xi}\|_2^2 \tag{6}$$

where $\|\,.\,\|_2^2$ is the Euclidean distance, and the minimum of such function is the variance. Therefore, the concepts can be extended to manifolds, provided that they do have a distance. In such case, the average is the point on the manifold minimizing

$$min_{\bar{\xi}\in\mathcal{M}}\frac{1}{N}\sum_{n=1}^{N}d(\xi_n,\bar{\xi})^2 \tag{7}$$

for d the distance in the manifold $\mathcal{M}$. The extension of the arithmetic mean to manifolds is called the Frechet mean.[22] The Frechet mean can be obtained using the exponential map which, in the case of (S^{2+}) is given in terms of angular differences.

Let $\bar{\xi}$ be the point we want to compute the exponential map and $\bar{\xi}_n=\bar{\xi}/\|\bar{\xi}\|$ the associated unitary vector. The inverse of the exponential map[12] projects maximum circles through $\bar{\xi}$ to its perpendicular vector, $\bar{\xi}_n^{\perp}$, on the tangent plane (see Fig.3). By general theory of Lie groups the exponential map is a local isometry. In the particular case of spheres,[12] it is an isometry between the circle and the vector space generated by $\bar{\xi}_n^{\perp}$ given by the angle, θ, between $\bar{\xi}_n$ and any point ξ in the maximum circle (see Fig.3):

$$\exp^{-1}:\xi\longmapsto\theta\bar{\xi}_n^{\perp}\qquad\bar{\xi}_n^{\perp}=\frac{\xi-\langle\xi,\bar{\xi}_n\rangle}{\|\xi-\langle\xi,\bar{\xi}_n\rangle\|}\quad\theta=\arctan\left(\frac{\langle\xi,\bar{\xi}_n^{\perp}\rangle}{\langle\xi,\bar{\xi}_n\rangle}\right) \tag{8}$$

Descriptive statistics are computed following.[12] Regarding the modes of variation, since $\exp^{-1}(\xi)$ are on a plane, the covariance matrix always has a zero eigenvalue corresponding to the direction perpendicular to the plane $\bar{\xi}_n$. The remaining modes are in terms of the local reference (2) and can be anatomically interpreted.

3. RESULTS

We have used the NPD framework for the creation of an anatomic atlas jointly modelling the gross anatomy and the fiber architecture of the LV using the 8 normal canine hearts. DTI volumes used in this work were acquired and processed by Drs. Patrick A. Helm and Raimond L. Winslow at the Center for Cardiovascular Bioinformatics and Modeling and Dr. Elliot McVeigh at the National Institute of Health (available at http://`www.ccbm.jhu.edu/`).

The gross anatomy has been obtained parameterizing the LV volume of each canine. B-Spline based parametric maps have been computed using $8\times8\times4$ control points. Using these control points a PDM has been built. In order to properly describe the variability observed in the 8 canine hearts, the 6 first modes of variation (which explain a 99.25% of the total shape variability) have been taken into account. Figure 4 shows the first 6 modes of variation for the gross anatomy. Each mode (shown in rows) is sampled in the range ±2 standard deviations from the average anatomy, shown in the central column.

In order to model the fiber architecture, DTI volumes containing the components of the first eigenvector were considered. Using the differential of the parametric map, the components of the eigenvectors were moved to Ω^3. Next, they were normalized and reoriented. At each point in Ω^3, statistical analysis, using the Frechet mean was applied to the 8 vectors (lying on S^{2+}). In order to compensate for the low number of DTI studies, we increased the number of samples by considering vectors in a 4-connected neighborhood defined in the circumferential-longitudinal plane (of Ω^3). This strategy allowed to increase up to 5 times the number of samples for computing the statistics, while avoiding to mix fiber orientations between different radial layers (where gradients of fiber variations are higher). The average model of the myocardial fibers is shown in Figure 5 where their orientation is visualized in Ω^3 considering different slices for fixed radial parameters, $w=\{0,0.21,0.35,0.64,0.78,1\}$ (for $w=0$ the endocardium and $w=1$ the epicardium). Images are given in the circumferential and longitudinal directions of Ω^3. The yellow lines represent the junction between right and left ventricles at anterior (continuous line) and posterior (dashed line) walls. Apical area is labelled 'A', basal 'B' and septal 'S'. We can observe

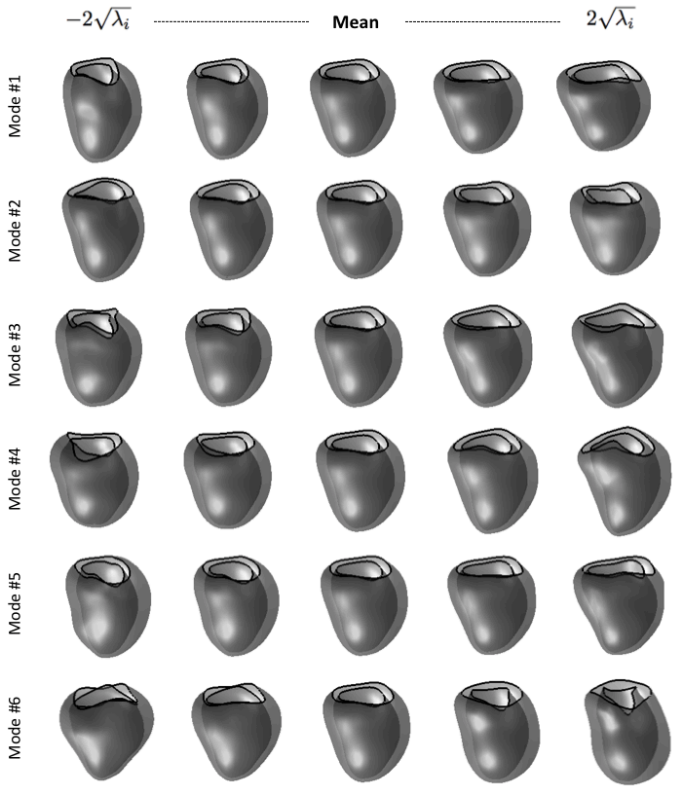

Figure 4. By rows, the 6 principal modes of variation obtained moving the model parameters up to ± 2 standard deviations from the mean, shown in the central column.

that endocardial and epicardial cuts present an approximate uniform fiber orientation with opposite sign with respect to the circumferential direction (each orientation is colored by cyan and magenta). We observe that as the radial parameter evolves from 0 to 1 (endocardium to epicardium), the orientation of fibers suffer from an abrupt change in orientation. Notice that this change starts at septal area and gradually propagates to rest of the tissue.

The joined model of the gross anatomy and the fiber architecture is obtained by mapping the fiber average model to the average geometry. This is achieved by applying the Differential of the average parametrization to the mean fibers computed in Ω^3. Figure 6 shows the average fibers over the average gross anatomy. The colors (cyan and magenta) are in concordance with those in Fig. 5 and the yellow curves stand for the RV-LV junctions at anterior wall (continuous) and inferior wall (discontinuous).

4. CONCLUSIONS

Up to our knowledge, current models just focus on one of the following anatomical aspects of the LV: the gross anatomy or the fiber architecture. We have used a Differential Geometry approach to define a mathematical framework (NPD) allowing to gather two different concepts, namely geometry and registration. This framework is well suited for modelling both, the gross anatomy and the fiber architecture. The first is modelled in the continuous domain by statistical analysis of manifold parametrizations using B-Spline formulation. This allows to linearize statistics (PDM) in the infinite dimensional space of differentiable functions. Fiber architecture is modelled using Riemmanian metrics given by angular differences.

As in[23] we have found evidence of two populations presenting opposite orientations, although we have not observed a concentric sheet disposition on the whole volume of the LV. Epicardium and endocardium might be considered as two layers oriented in opposite directions. As we approach the mid-wall, this uniformity in fiber

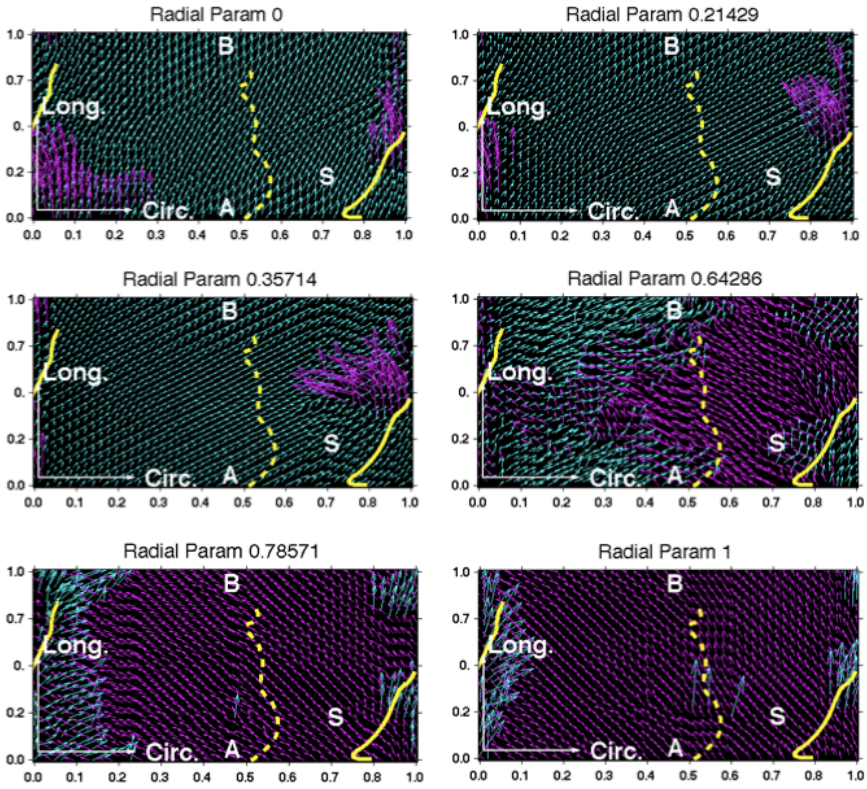

Figure 5. Average fiber distribution in Ω^3 for 6 slices of constant radial parameter $w = \{0, 0.21, 0.35, 0.64, 0.78, 1\}$, for $w = 0$ the endocardium and $w = 1$ the epicardium. The yellow lines represent the junction between right and left ventricles at anterior (continuous line) and posterior (dashed line) walls. Apical area is labelled 'A', basal 'B' and septal 'S'.

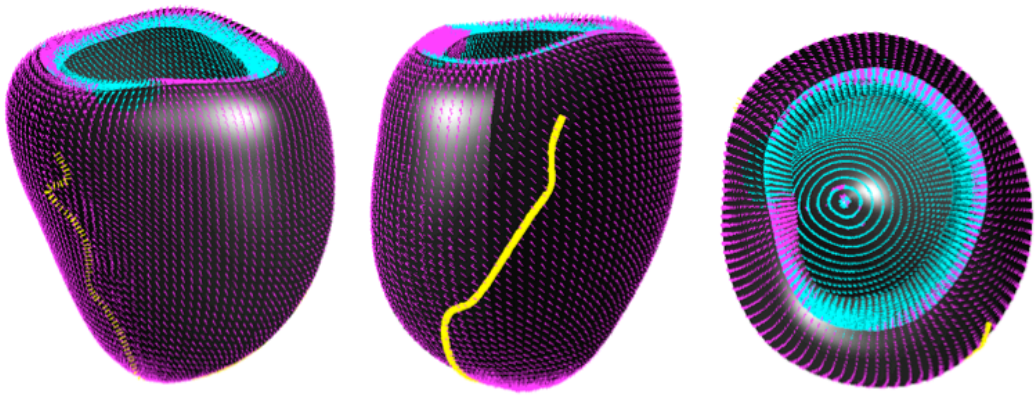

Figure 6. verage fiber architecture over the average gross anatomy of the $\mathcal{LV}$. The colors (cyan and magenta) are in concordance with those in Fig. 5.

orientations turns into two clusters of opposite oriented fibers. This suggests that at mid-wall bundles of fibers with opposite directions entangle.

This non-laminar behavior might be an evidence of a complex structure (maybe helicoidal as suggested by[24]) of fibers in space.

REFERENCES

[1] Cootes, T., Taylor, C., Cooper, D., , and Graham, J., "Active shape models - their training and application," *Computer Vision and Image Understanding* **61**, 38–59 (1995).

[2] Frangi, A., Rueckert, D., Schnabel, J., and Niessen, W., "Automatic construction of multiple-object three-dimensional statistical shape models: application to cardiac modeling," *Medical Imaging, IEEE Transactions on* **21**(9), 1151–1166 (2002).

[3] Davis, B., Fletcher, P., Bullitt, E., and Joshi, S., "Population shape regression from random design data," in [*Computer Vision, 2007. ICCV 2007. IEEE 11th International Conference on*], 1–7 (2007).

[4] Helm, P., *A novel technique for quantifying variability of cardiac anatomy: Application to the dyssynchronous failing heart*, PhD thesis, Johns Hopkins Univ., Baltimore (2005).

[5] Gilbert, S., Benson, A., Li, P., and "et al.", "Regional localization of the left ventricular sheet structure: integration with current models of cardiac fiber, sheet an band structure.," *Eur. J. Card-thor. Surg.* **32**, 231–249 (2007).

[6] Taccardi, B., E. Macchi, R. L., and Ershler, P., "Effect of myocardial fiber direction on epicardial potentials," *Circulation* **90**, 3076–3090 (1994).

[7] Wickline, S., Verdonk, E., Wong, A., and et al., "Structural remodeling of human myocardial tissue after infarction. quantification with ultrasonic backscatter," *Circulation* **85**, 259–268 (1992).

[8] Sermesant, M., Delingette, H., and Ayache, N., "An electromechanical model of the heart for image analysis and simulation," *Medical Imaging, IEEE Transactions on* **25**(5), 612–625 (2006).

[9] Scollan, D., Holmes, A., Wilson, R., and "et al.", "Histological validation of myocardial microstructure obatined from diffusion tensor imaging," *Am. J. Phys.- Heart and Circ. Phys.* **275**, 2308–2318 (1998).

[10] Geerts, L., Bovendeerd, P., Nicolay, K., and Arts, T., "Characterization of the normal cardiac myofiber field in goat measured with mr-diffusion tensor imaging.," *Am. J. Physiol.* **283**, H139–H145 (2002).

[11] Peyrat, J.-M., Sermesant, M., Pennec, X., and "et al.", "A computational framework for the statistical analysis of cardiac diffusion tensors: application to a small database of canine hearts," *IEEE Trans. Med. Imag.* **26(10)**, 1500–1514 (2007).

[12] Pennec, X., Fillard, P., and Ayache, N., "A riemmanian framework for tensor computing," *Int. J. Comp. Vis.* **66(1)**, 41–66 (2006).

[13] Spivak, M., [*A Comprehensive Introduction to Differential Geometry, vol. 1*], Publish or Perish, Inc (1999).

[14] Garcia-Barnes, J., Gil, D., Pujadas, S., Carreras, F., and Ballester, M., "A normalized parametric domain for the analysis of the left ventricle function," in [*3rd Int. Conf. Comp. Vis. Theory App.*], 267–274 (2008).

[15] Garcia-Barnes, J., Gil, D., Badiella, L., Hernandez-Sabate, A., Carreras, F., Pujades, S., and Marti, E., "A normalized framework for the design of feature spaces assessing the left ventricular function," *Medical Imaging, IEEE Transactions on* (2010). In Press.

[16] LeGrice, I., Hunter, P., and Smaill, B., "Laminar structure of the heart: a mathematical model," (1997).

[17] Gower, J., [*Generalized procrustes analysis*], Phychometrika (1975).

[18] Moakher, M., "A differential geometry approach to the geometric mean of symmetric positive-defined matrices," *SIAM-J.Mat. Ana. App.* **26(3)**, 735–747 (2005).

[19] Arsigny, V., Fillard, P., Pennec, X., and et al., "Log-euclidean metrics for fast and simple calculus on diffusion tensors," *Mag. Res. Med.* **56(2)**, 411–421 (2006).

[20] Arsigny, V., Fillard, P., Pennec, X., and et al., "Log-euclidean metrics for fast and simple calculus on diffusion tensors," *Mag. Res. Med.* **56**(2), 411–421 (2006).

[21] Moakher, M., "A differential geometry approach to the geometric mean of symmetric positive-defined matrices," *SIAM-J.Mat. Ana. App.* **26(3)**, 735–747 (2005).

[22] Pennec, X., "Intrinsic statistics on riemannian manifolds - basic tools for geometric measurements," *Journal of Mathematical Imaging and Vision* **25**, 127–154 (2006).

[23] Helm, P., Beg, M., Miller, M., and et al., "Measuring and mapping cardiac fiber and laminar architecture using diffusion tensor mr imaging," *Annals of the New-york Accademy of Science* **1047**, 296–307 (2005).

[24] Ballester, M., Ferreira, A., and Carreras, F., "The myocardial band," *Heart Failure Clinics* **4**, 261–272 (2008).